Available online at www.sciencedirect.com
SCIENCE DIRECT®
Journal of Power Sources 125 (2004) 199–205
JOURNAL OF POWER SOURCES
www.elsevier.com/locate/jpowsour

Silver: high performance anode for thin film lithium ion batteries

G. Taillades*, J. Sarradin

Laboratoire de Physicochimie de la Matière Condensée, UMR CNRS 5617, Université Montpellier II, Place E. Bataillon, 34095 Montpellier Cedex 5, France

Received 21 February 2003; received in revised form 4 July 2003; accepted 28 July 2003

Abstract

Among metals and intermetallic compounds, silver exhibits a high specific capacity according to the formation of different Ag–Li alloys (up to $AgLi_{12}$) in a very low voltage range versus lithium (0.250–0 V). Electrochemical results including Galvanostatic Intermittent Titration Technique (GITT) as well as cycling behaviour experiments confirmed the interesting characteristics of silver thin film electrodes prepared by radio frequency (r.f.) sputtering.

XRD patterns recorded at different electrochemical stages of the alloying/de-alloying processes showed the complexity of the silver–lithium system under dynamic conditions. Cycling life depends on several parameters and particularly of the careful choice of cut-off voltages. In very well monitored conditions, galvanostatic cycles exhibited flat reversible plateaus with a minimal voltage value (0.050 V) between charge and discharge, a feature of great interest in the use of an electrode. The first results of a lithium ion battery with both silver and $LiMn_{1.5}Ni_{0.5}O_4$ thin films are presented.

Keywords: Alloy; Ag–Li; Thin films; Lithium ion batteries

1. Introduction

Advances in the microelectronics industry have strongly reduced the power required to supply energy for electronic devices. As a consequence, thin film-based microbatteries have been developed as power sources for devices such as smart cards, electronic coding, MEMS as well as CMOS-based integrated circuits.

Lithium metal thin films in association with cathodic materials such as $LiCoO_2$ [1], TiS_2 [2], TiO_yS_z [3] and V_2O_5 [4,5] were initially used as the negative electrode since this metal is a very attractive material for the obtention of high voltage batteries. The main drawbacks of lithium metal are corrosion and dendrite formation on the negative side resulting in poor cycling efficiency and cell shorting. To overcome these problems, other negative microelectrodes were investigated. Goldner et al. [6] were the first to develop an all solid state lithium ion battery with carbon-based thin films as the anode. Similar investigations were carried out by Levasseur and coworkers [7] on graphite multilayer thin films. The drawback connected to the carbon thin film concerns the difficulty to obtain the desired nature of the deposit.

However, the announcement by Fuji Photo Film Co. of a new amorphous oxide anodic material that can store twice the reversible capacity of carbonaceous materials led to a new approach [8]. The concept of Tin Composite Oxide (TCO) consisted in an in situ buffer able to accommodate mechanical stresses experienced by the Li–Sn alloying/de-alloying processes. Simultaneously, much effort has been made to prepare thin layers of tin-based compounds. Among them, tin nitride [9], tin oxynitride [10], tin dioxide [11], Sn–Cu alloys [12] as well as TCOs [13] were studied. In our work on the latter material, thin films were prepared from a composite target ($Sn/SnB_{0.6}P_{0.4}O_{2.9}$). The first objective was to obtain thin films with similar electrochemical capacities as previously announced for bulk material. The second was to increase the tin amount in the thin film and consequently the specific capacity since the electrochemical yield is the result of Li–Sn alloying/de-alloying processes [14]. The main drawback was that the anodic material was connected to the Li_2O formation during the first charge (uptake of lithium). Consequently, the charge/discharge efficiency of the first cycle is low and the additional problem of volume expansion prevents these anodic materials from being adopted as negative electrodes in lithium ion batteries. Nevertheless, the fact that the high reversible capacity of TCO materials was due to the Li–Sn alloying/de-alloying

* Corresponding author. Tel.: +33-4-67-14-32-03; fax: +33-4-67-14-42-90.
E-mail address: gilles@lpmc.univ-montp2.fr (G. Taillades).

0378-7753/$ – see front matter © 2003 Elsevier B.V. All rights reserved.
doi:10.1016/j.jpowsour.2003.07.004

processes renewed interest for lithium alloys as anodic materials.

Lithium alloys have been studied for an even longer time than carbonaceous materials for this application. The first studies involved Li–Al alloys in molten salt electrolytes [15] and later a number of other binary or ternary alloys [16–18] and intermetallic compounds [19] were examined. An obvious advantage of the lithium alloys concerns their huge volumetric charge densities. Unfortunately, following lithium uptake the volume change may be very large and close to a factor of two or three well greater than carbon (only 10%). The thin film concept which minimizes the volume change effect is well suited for the use of lithium alloys. Twenty years ago [20], thin layers of lithium alloys were already cycled with high efficiencies. Moreover, many metals including noble metals such as gold and silver can be alloyed with lithium. According to the thickness of thin layers (1000–3000 Å), it is not unrealistic to use noble metal deposits economically viable in the microelectronics industry.

Looking for metal-based lithium alloys, silver was chosen for three major advantages. One is the very high specific capacity related to the ultimate $AgLi_{12}$ composition [21].The other is that the alloying/de-alloying processes occur in a very low voltage range (0.250–0 V) compared to the Li–Sn system minimizing the reduction in the cell voltage. The last but not least concerns the preparation of thin layers, easily obtained either by thermal evaporation or radio frequency (r.f.) sputtering.

2. Experimental

Silver thin films were deposited onto stainless steel substrates (area: 1.5 cm^2) by radio frequency (r.f.) sputtering under argon plasma using a silver target (Johnson Matthey 2 in. diameter, 0.125 in. thick). Compared to thermal evaporation, the r.f. sputtering offers better adherence of the deposited layers as well as an easy monitoring of the thickness.

A Dektak 3 profilometer was used to rapidly measure the thickness of the deposits. SEM (Cambridge 360) also allows the thickness of metallic films to be measured and the surface aspect to be observed. The mass of the silver thin layer calculated from the thickness (1000 Å) and the assumed density (10.5 g/cm^3) is close to 0.1 mg/cm^2. Air sensitive silver–lithium thin films were embedded in small polyethylene bags within a glove box and immediately thereafter checked using a Seifert θ–θ diffractometer with a Cu target X-ray tube and a diffracted beam monochromator.

Samples were checked at different electrochemical stages of the alloying/de-alloying processes. To investigate the electrochemical behaviour, a Mac Pile II from Bio-Logic was used. Galvanostatic charge/discharge curves as well as Galvanostatic Intermittent Titration Technique (GITT) were performed on silver thin films as the working electrode. A lithium disk (Aldrich) was used as both the counter and reference electrodes. The electrolyte (1 M $LiPF_6$-EC-PC-DMC) was supported by a porous fibre glass separator (Millipore). All electrochemical measurements were carried out in an argon filled dry glove box where the H_2O content was kept below 1 ppm.

3. Results and discussion

Electrochemical results previously published [22] with TCO thin films mentioned a gold collector contribution to the faradaic yield and it was interesting to check out the electrochemical behaviour of metallic thin films as anodic material. Only a few metals including silver are able to both form alloys with a high lithium percentage and be electrochemically active at very negative potentials. At this point, it is important to first consider equilibrium or near-equilibrium conditions. The quantitative results obtained under dynamic conditions deviated from capacities which can be calculated by the use of thermodynamic principles. On one hand, the results obtained under dynamic conditions depend on experimental parameters (e.g. current density) and on the other hand, the faradaic yields may be somewhat representative of a general current use. However, only the near-equilibrium situation has to be considered for comprehensive change in composition of the electrode.

We have used a Galvanostatic Intermittent Titration Technique (GITT). This method allows to distinguish single phase from two phase domains. Briefly, a two phase mixture will give rise to a plateau in the curve and for a single phase domain, the potential which depends upon the state of charge, i.e. the amount of lithium, will decrease. The Ag–Li equilibrium diagram [21] is somewhat complex and few data have been published [23,24]. In addition to the terminal solid solutions, four intermediate phases, denoted respectively, β, γ_3, γ_2, and γ_1 have been observed. Silver thin layers were checked during the alloying process and an experimental curve obtained by GITT is shown in Fig. 1. Some transitions between plateaus and slopes are missing or sometimes difficult to distinguish. At room temperature, the solubility of lithium in silver which extends to a value of 46.6 at.% ($x = 0.87$), i.e. the α solid solution was easily observed in Fig. 1. Over 46.6 at.% a narrow area which corresponds to a two phase domain ($\alpha + \beta$) appears between 46.6 and 51 at.% ($x = 1.04$). Neither the resulting plateau and the slope due to the single AgLi β phase extending from 51 to 56 at.% ($x = 1.27$), nor the discontinuity between their respective domains were observed in the GITT curve. The dotted line reported in Fig. 1 with an abscissa value $x = 1.27$ is relevant to the theoretical limit of the single Ag–Li β phase domain. With further increase in lithium content, a two phase area ($\beta + \gamma_3$) occurs from 56 to 63.5 at.% ($x = 1.74$). The transition with the former domain was indistinguishable but a quasi plateau corresponding to this two phase domain ($\beta + \gamma_3$) might be observed. The γ_3 (Ag_4Li_9) single phase domain is very wide (63.5–73 at.%) and clearly appears in

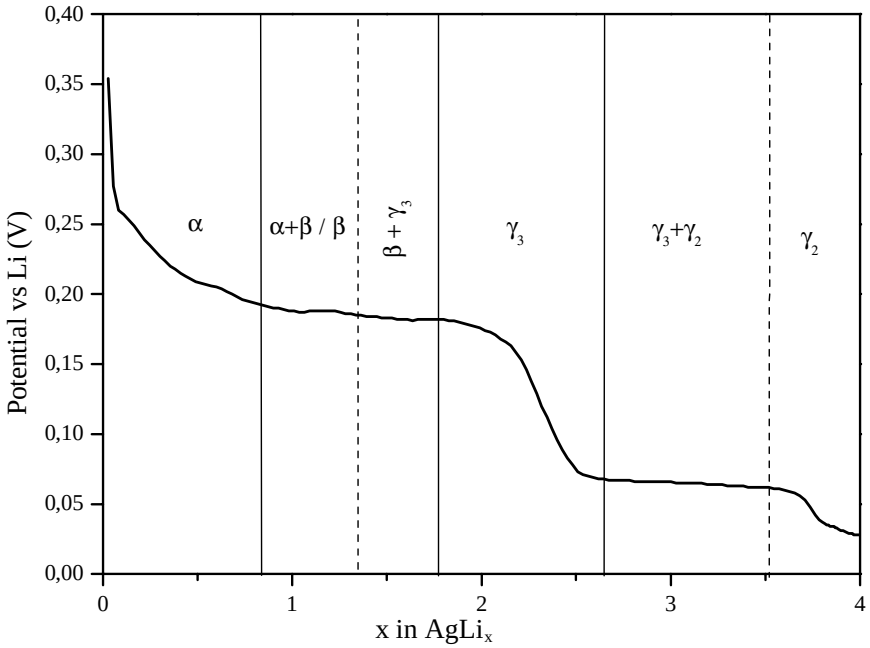

Fig. 1. Titration curve of a silver thin film electrode during alloying process. Pulse duration: 0.1 h; pulse intensity: 15 μA; open circuit potential time derivative: 5 mV/h.

the curve since the potential drop is close to 0.120 V. Over 73 at.% lithium ($x = 2.7$) the ($\gamma_3 + \gamma_2$) two phase domain is followed by a γ_2 single phase based on the Ag_3Li_{10} composition. In fact, the two phase domain ($\gamma_3 + \gamma_2$) lies well over its theoretical limit ($x = 3.2$). The experimental boundary (dotted line) was close to $x = 3.5$ before the beginning of the γ_2 phase domain was observed. The region from 83 to 100 at.% lithium was not investigated since the GITT experiment stopped at the $AgLi_4$ composition. A γ_1 phase with an ultimate $AgLi_{12}$ composition exists at room temperature from approximately 87 to 93 at.% lithium. Among all the phases described in the above paragraph,

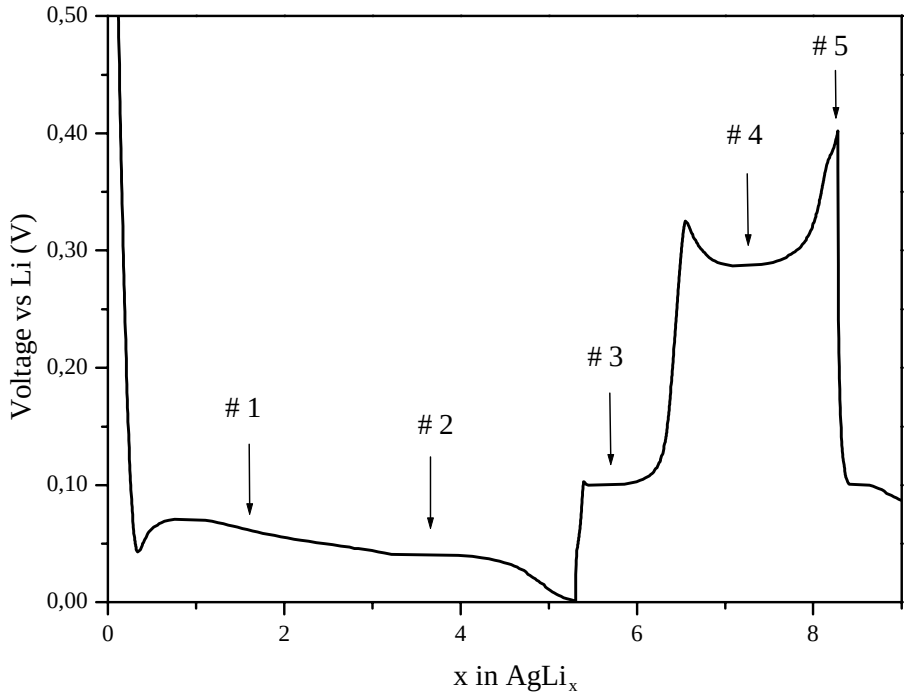

Fig. 2. First charge/discharge cycle of a silver thin film electrode. Current density: 50 μA/cm^2; voltage window: 0.4–0 V vs. Li; electrode area: 1.5 cm^2. Digits #1–5 refer to the compositions checked out by XRD.

only the β phase diffraction peaks were identified (JCPDS 4-805).

When the overall composition of the Ag–Li alloy is caused to change as the result of the passage of very low current or even during GITT experiment, equilibrium may depend on the nucleation rate of the different phases [25]. Since the GITT experiment was performed with an open circuit time derivative less than 5 mV/h, one can think that the equilibrium is not actually attained and as a consequence not all phases which are present in the phase diagram may be formed. Nevertheless, the titration curve allowed to distinguish the major changes between the different phase domains electrochemically observed in this study.

The curve obtained under dynamic electrochemical conditions was quite different from the titration curve. Silver thin film electrodes were studied in an alloying/de-alloying voltage ranging from 0.400 to 0 V versus lithium. The first charge/discharge cycle (Fig. 2) showed two pseudo plateaus at 0.060 and 0.040 V versus lithium during the alloying process while de-alloying occurred at 0.100 and 0.300 V versus lithium. In these conditions, the coulombic capacity during the uptake of lithium corresponds to a $AgLi_{5.2}$ alloy formula (84 at.% lithium). One can observe that alloying process is more extended than de-alloying process, evidencing different kinetics between them. Lithium diffusion effects giving rise to polarization/depolarization phenomena were also observed at the beginning of both stages #1 and #4. Nevertheless, it was interesting to check out by means of XRD the thin film electrodes at different stages of the alloying/de-alloying processes since the dynamic electrochemical conditions are close to practical use. Diffraction patterns obtained from stages #1 to #5 are reported in Fig. 3 as well as the standard diffraction pattern of silver (JCPDS 4-783). An unknown phase called I appeared as soon as plateau #1 and was always observed in stage #5. At stage #5, de-alloying process is quasi-ended. Only the phase I which still appears is considered as an irreversible phase. That phase might explain the yield difference between charge and discharge. The AgLi phase (JCPDS 4-805) was clearly detected from plateaus #2 to #4. This latter phase is reversible as well as the phase called II undetected in stage #5. Finally, in these experimental conditions, electrochemical behaviour during the alloying/de-alloying processes should implied two reversible phases (AgLi, phase II) and one irreversible phase (phase I).

Looking at the charge/discharge curves of the silver-based thin film electrode, the research of the most convenient electrochemical window was necessary in order to obtain both interesting cycleability and reliability. The choice of the charge/discharge cut-off voltage values is crucial since during cycling mechanical stress and cracks are induced in connection with the drastic volume change related to uptake/release of lithium. Four electrochemical windows were investigated using the same current density value (50 μA/cm^2). Experimental results are reported in Fig. 4. The choice of cut-off voltages ranging from 0 to 0.400 V versus lithium (choice #1) gave rise to a drastic capacity fading after 25 cycles. This electrochemical window corresponded to a quasi full charge/discharge of the thin film electrode in our experimental conditions. Limiting the lower value to 0.050 V versus lithium (choice #2) strongly reduced the amount of lithium able to form alloys with silver. As a consequence, capacity decreased compared to choice #1 and cycling ability was even worse. Obviously, the choice of 0.400 V versus lithium as the discharge cut-off voltage was not judicious all the more that two plateaus were involved during the de-alloying process. The choice #3 using 0.200 V instead of 0.400 V allowed the discharge to be performed with only one plateau while keeping 0 V versus lithium as the low cut-off voltage. Kinetics problems occurred since capacity was improved before decreasing after 75 cycles. At this point, modifying the charge voltage cut-off was necessary. Following several runs, a mid value (0.015 V versus lithium) was retained allowing the charge to be nearly entire. Simultaneously, the discharge was stopped at 0.150 V versus lithium. In these conditions, cycling ability was much better (150 cycles). Finally, the achievement of both a high cycleability and good reversible specific capacity required to carefully choose the charge/discharge cut-off voltage values.

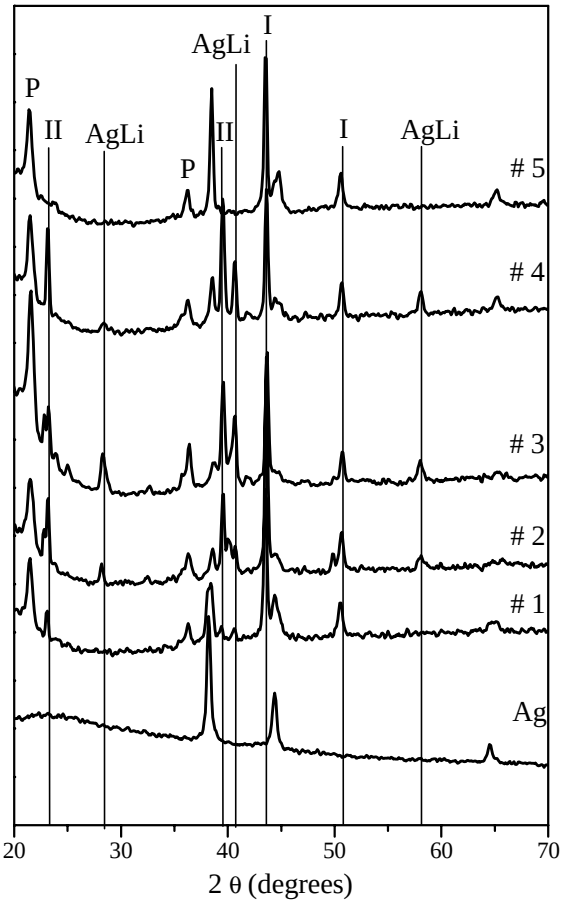

Fig. 3. XRD patterns evolution of silver thin film electrodes at different stages of the alloying/de-alloying processes. P: polyethylene protective film; I: phase I; II: phase II.

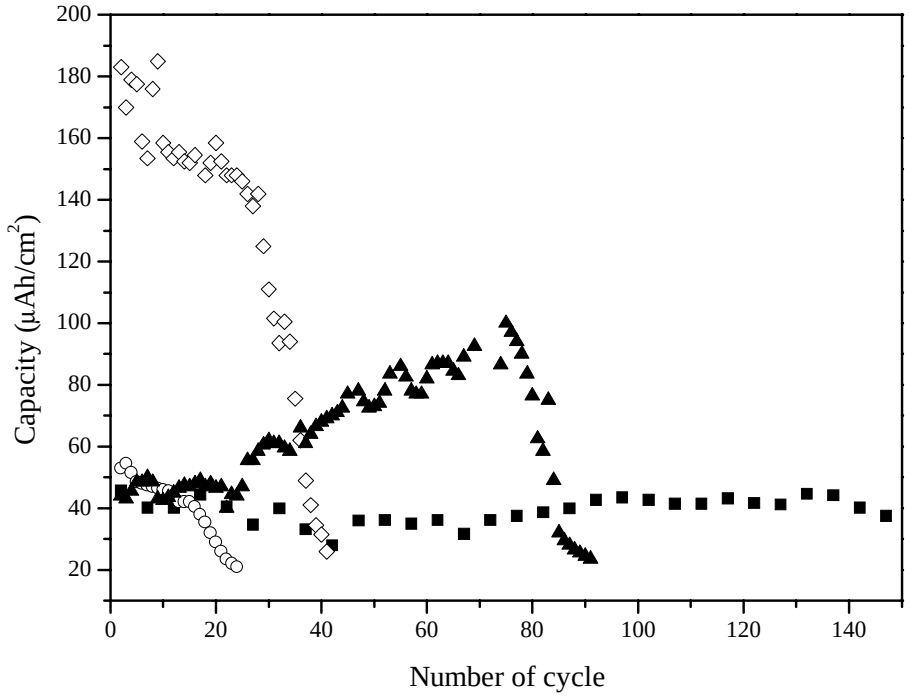

Fig. 4. Effect of cut-off voltage values on cycling ability of silver thin film electrodes. Current density: 50 μA/cm²; electrode area: 1.5 cm²; voltage windows vs. Li. (◇) 0.400–0 V; (○) 0.400–0.050 V; (▲) 0.200–0 V; (■) 0.150–0.015 V.

Thin film electrodes (1000 Å thick) were checked using the optimized cut-off voltage values. An outstanding feature concerned the galvanostatic cycles which exhibited flat reversible plateaus with a minimal voltage value (0.060 V) between the charge and the discharge as shown in Fig. 5. Curves presented were obtained at 25 μA/cm² and faradaic yields between charge and discharge are well balanced. Moreover, compared to other lithium alloys (e.g. Li–Sn), the very negative and narrow voltage window strongly limit the reduction in the cell voltage.

Current density effect on electrochemical behaviour was studied. A run of galvanostatic charge/discharge cycles was

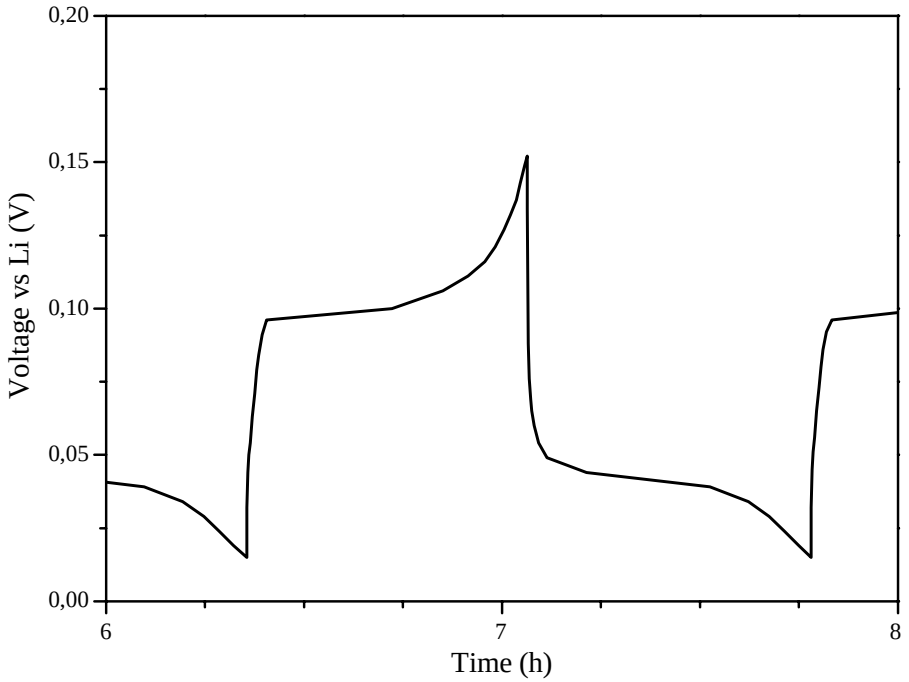

Fig. 5. Charge/discharge cycle of a silver thin film electrode. Current density: 25 μA/cm²; voltage window vs. Li: 0.150–0.015 V; electrode area: 1.5 cm².

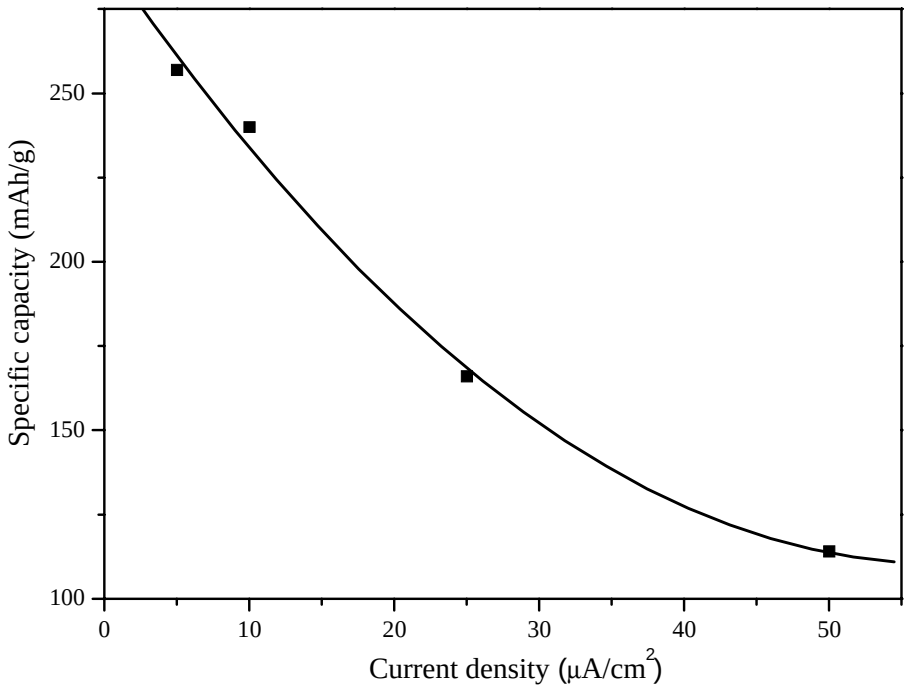

Fig. 6. Current density effect on specific capacity of silver thin film electrodes. Voltage window: 0.150–0.015 V vs. Li; deposits thickness: 1000 Å; electrodes area: 1.5 cm^2.

performed with thin film electrodes using current densities in the 5–50 $\mu A/cm^2$ range. The effect of current density on specific capacity of the thin film electrodes is reported in Fig. 6. When current density increased 10 times (5–50 $\mu A/cm^2$) the specific capacity was divided in two. The corresponding charge/discharge rates at 5 and 50 $\mu A/cm^2$ were *C*/5 and 3*C*, respectively. One can think that the electrochemical behaviour of the silver-based thin film electrodes is the result of a given set of definite conditions in connection with:

1. A first uptake of lithium well over the amount released during the discharge.

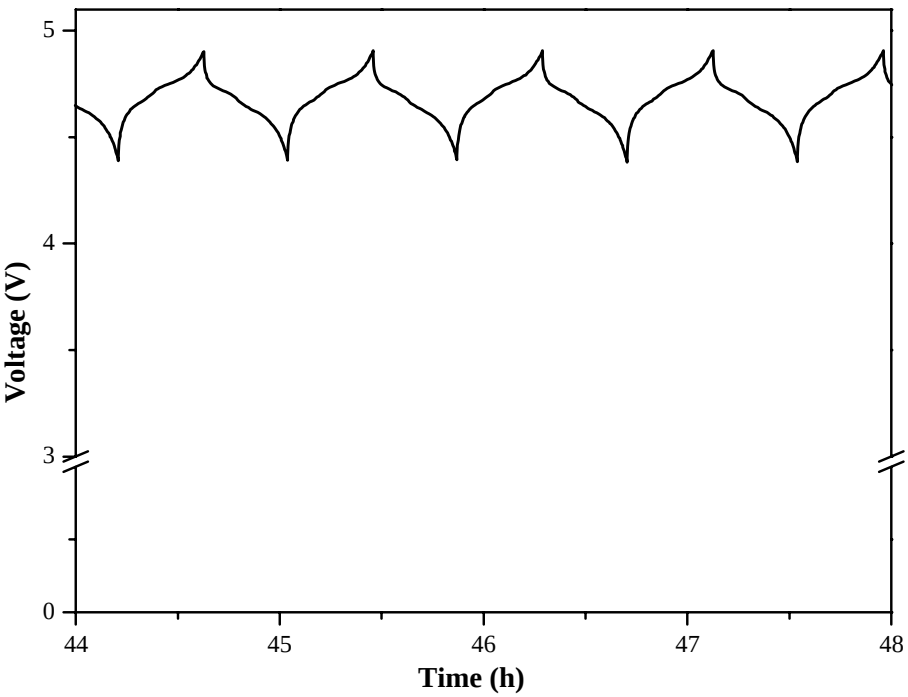

Fig. 7. Charge/discharge cycles of an Ag thin film/1 M $LiPF_6$-EC-PC-DMC/$Li_{1.2}Mn_{1.5}Ni_{0.5}O_4$ thin film microbattery. Current density: 25 $\mu A/cm^2$; electrodes area: 1.5 cm^2; charge/discharge cut-off voltages: 4.9 V/4.4 V.

2. The use of the thin film electrode as a lithium reservoir buffered from mechanical stress since lithium amounts involved during the charge/discharge processes were deliberately reduced.
3. The choice of judicious cut-off voltages allowing the use of the same phase mixtures during the charge/discharge processes.
4. The thin film concept.

In order to finalize this study a silver based thin film anode was associated to a 5 V $Li_{1.2}Mn_{1.5}Ni_{0.5}O_4$ thin film cathode [26] in a $LiPF_6$-EC-PC-DMC electrolyte. A capacity close to 25 $\mu Ah/cm^2$ over 1000 cycles at an average working voltage of 4.65 V was obtained. Charge/discharge cycles are shown in Fig. 7.

4. Conclusion

The thin film concept which minimizes the volume change effect was developed to elaborate metal-based electrodes. Sputter deposited silver thin layers were studied as a new anodic material for thin film lithium ion batteries. XRD diffraction patterns performed on thin film electrodes at different stages of the electrochemical alloying/de-alloying processes showed existence of phase mixtures including the AgLi intermetallic compound.

An appropriate choice of the cut-off voltage values during charge/discharge cycles gave rise to an interesting electrochemical behaviour. Galvanostatic cycles exhibit flat reversible plateaus at low potentials versus lithium with a minimal voltage value between the charge and the discharge.

References

[1] J.B. Bates, N.J. Dudney, B. Neudecker, A. Ueda, C.D. Evans, Solid State Ion. 135 (2000) 33.
[2] S.D. Jones, J.R. Akridge, J. Power Sources 54 (1995) 63.
[3] M. Martin, F. Faverjon, Thin Solid Films 398–399 (2001) 572.
[4] R. Creus, J. Sarradin, R. Astier, A. Pradel, M. Ribes, Mater. Sci. Eng. B3 (1989) 109.
[5] E.J. Jeon, Y.W. Shin, S.C. Nam, W. Cho, Y.S. Yoon, J. Electrochem. Soc. 148 (2001) A 318.
[6] R.B. Goldner, T.Y. Liu, S. Slaven, A. Gerouki, P. Zerigian, T.E. Haas, F.O. Arntz, S. Jones, Electrochem. Soc. Proc. 95 (22) (1996) 173.
[7] M. Hess, E. Lebreau, A. Levasseur, J. Power Sources 68 (1997) 204.
[8] Y. Idota, T. Kubota, A. Matsufuji, Y. Maekawa, T. Miyasaka, Science 276 (1997) 1395.
[9] K.S. Park, Y.J. Park, M.K. Kim, J.T. Son, H.G. Kim, S.G. Kim, J. Power Sources 103 (2001) 67.
[10] B.J. Neudecker, R.A. Zuhr, J.B. Bates, J. Power Sources 81–82 (1999) 27.
[11] T. Brousse, R. Retoux, U. Herterich, D.M. Schleich, J. Electrochem. Soc. 145 (1998) 1.
[12] N. Tamura, R. Ohshita, M. Fujimoto, S. Fujitani, M. Kamino, I. Yonezu, J. Power Sources 107 (2002) 48.
[13] J. Sarradin, N. Benjelloun, G. Taillades, M. Ribes, J. Power Sources 97–98 (2001) 208.
[14] I.A. Courtney, J.R. Dahn, J. Electrochem. Soc. 144 (1997) 2045.
[15] E.C. Gay, D.R. Vissers, F.J. Martino, K.E. Anderson, J. Electrochem. Soc. 123 (11) (1976) 1591.
[16] C.J. Wen, B.A. Boukamp, R.A. Huggins, W. Weppner, J. Electrochem. Soc. 126 (12) (1979) 2258.
[17] J. Wang, I.D. Raistrick, R.A. Huggins, J. Electrochem. Soc. 133 (3) (1986) 457.
[18] M. Wachtler, M. Winter, J.O. Besenhard, J. Power Sources 105 (2002) 151.
[19] M.M. Thackeray, J.T. Vaughey, C.S. Johnson, A.J. Kropf, R. Benedek, L.M.L. Fransson, K. Edstrom, J. Power Sources 113 (2003) 124.
[20] M. Garreau, J. Thevenin, M. Fekir, J. Power Sources 9 (1983) 235.
[21] T. Massalski, CD ROM: Binary Alloy Phase Diagrams, ASM International, OH, USA, 1996.
[22] G. Taillades, N. Benjelloun, J. Sarradin, M. Ribes, Solid State Ion. 152–153 (2002) 119.
[23] W.E. Freeth, G.V. Raynor, J. Inst. Met. 82 (1954) 569.
[24] P. Villars, L.D. Calvert, Pearson's Handbook of Cristallographic Data for Intermetallic Phases, vol. 1, 1991, p. 587.
[25] R.A. Huggins, J. Power Sources 81–82 (1999) 13.
[26] P. Soudan, T. Brousse, G. Taillades, J. Sarradin, in: Proceedings of the 203rd Meeting of the Electrochemical Society, Paris, April 2003.